X-ray Sensitive Material

by
M. Joseph Roberts
and
Curtis E. Johnson
Chemistry Division
Research and Engineering Group

DECEMBER 2015

NAVAL AIR WARFARE CENTER WEAPONS DIVISION
China Lake, CA 93555-6100

FOREWORD

This report documents work carried out and completed in a series of small projects supported by Deputy Assistant Secretary of the Navy for Research, Development, Test, and Evaluation (RDT&E) from fiscal years 2011 through 2014. The research resulted in a composite material that holds a quasi-permanent electric charge and rapidly discharges the electric charge upon X-ray exposure.

S. FALLIS, *Head*
Chemistry Division
1 December 2015

REPORT DOCUMENTATION PAGE

1. REPORT DATE *(DD-MM-YYYY)*	2. REPORT TYPE	3. DATES COVERED (From - To)
01-12-2015	Final report	1 October 2010–30 September 2014

4. TITLE AND SUBTITLE

X-ray Sensitive Material (U)

5a. CONTRACT NUMBER
N/A

5b. GRANT NUMBER
N/A

5c. PROGRAM ELEMENT NUMBER
N/A

6. AUTHOR(S)

M. Joseph Roberts and Curtis E. Johnson

5d. PROJECT NUMBER
N/A

5e. TASK NUMBER
N/A

5f. WORK UNIT NUMBER
N/A

7. PERFORMING ORGANIZATION NAME(S) AND ADDRESS(ES)

Naval Air Warfare Center Weapons Division
1 Administration Circle
China Lake, California 93555-6100

8. PERFORMING ORGANIZATION REPORT NUMBER

NAWCWD TM 8772

9. SPONSORING/MONITORING AGENCY NAME(S) AND ADDRESS(ES)

Department of Navy
Deputy Assistant Secretary of the Navy for Research, Development,
Test, and Evaluation (RDT&E)

10. SPONSOR/MONITOR'S ACRONYM(S)

DASN/RDT&E

11. SPONSOR/MONITOR'S REPORT NUMBER(S)

N/A

12. DISTRIBUTION/AVAILABILITY STATEMENT

DISTRIBUTION STATEMENT A. Approved for public release.

13. SUPPLEMENTARY NOTES

None.

14. ABSTRACT

(U) This report is the culmination of a series of small projects from fiscal years 2011 through 2014. These projects sought a material that not only exhibited a measureable effect when dosed with X-rays (5 seconds using 80 to100 kilovolts [kV], 5 milliamperes [mA], tungsten [W] target) but could also withstand temperature extremes encountered during processing and potential application.

(U) The result of these efforts was a composite material that would hold a quasi-permanent electric charge and rapidly discharge the electric charge upon X-ray exposure. The composite material combined the properties of an electret and an X-ray photoconductor, with a measurable charge maintained for at least a period of hours and an X-ray response occurring within an increment of time that depended upon incident X-ray power.

15. SUBJECT TERMS

Composite, Electret, Ionizing Radiation, X-ray Photoconductor

16. SECURITY CLASSIFICATION OF:

a. REPORT	b. ABSTRACT	c. THIS PAGE
UNCLASSIFIED	UNCLASSIFIED	UNCLASSIFIED

17. LIMITATION OF ABSTRACT

SAR

18. NUMBER OF PAGES

30

19a. NAME OF RESPONSIBLE PERSON
M. Joseph Roberts

19b. TELEPHONE NUMBER *(include area code)*
(760) 939-1394

CONTENTS

ACKNOWLEDGMENTS

BACKGROUND

In fiscal year 2012 (FY12), a literature review of the previous 30 years was conducted to identify the approaches to X-ray detection. Much of this research was aimed toward the development of digital X-ray imaging. Although not the goal of our work, much was learned from these published reports. There were two main types of X-ray detection methods: "indirect," which uses a scintillation material coupled to a light detector, and "direct," which measures a change generated by the material upon exposure. Materials used for direct detection of X-rays include heavy metal halide compounds (lead(II) iodide [PbI_2], mercury(II) iodide [HgI_2], bismuth(III) iodide [BiI_3]) (References 1 and 2) and thallium bromide (TlBr) (Reference 3), inorganic semiconductors (silicon [Si], cadmium zinc telluride [CdZnTe]) (Reference 4) and selenium (References 5 and 6), Ne-Xe plasma (Reference 7), semiconducting organic polymers (Reference 8) and crystals (Reference 9), and bismuth oxide/semiconducting polymer composite (Reference 10).

Aside from the X-ray detector work, there were reports about materials affected by X-ray exposure. "Reduction of metal ions while recording XPS[*] data was reported" and appeared to be correlated with the reduction potential (References 11, 12, and 13). Other reports have used X-rays from a synchrotron source to deposit metals: gold (References 14 and 15) and titanium (Reference 16). X-rays have also been used to modify a cuprate superconductor (Reference 17). Of particular interest to us was the effect of X-rays on BiI_3/nylon nanocomposites (References 18 and 19). Nylon-11 is a commodity polymer that is melt-processable into injection-molded parts and extruded fibers. Nylon-11 is nontoxic and has very low solubility and high thermal stability (melting point around 200°C). BiI_3 imparts strong X-ray attenuation at relatively low cost (\$5 per gram [g] retail in 2011). The X-ray attenuation of BiI_3 is a function of X-ray photon energy (Reference 20). As can be seen in Figure 1, X-rays from a molybdenum (Mo) target would be more strongly attenuated than X-rays from a tungsten (W) target (Reference 21). The BiI_3/Nylon-11 nanocomposite material looked promising due to its reported ease of preparation, relatively low toxicity, and reported X-ray photoconductivity. However, information was lacking on the mechanism of X-ray photoconductivity, its persistence after X-ray exposure, and the quantitative effect of X-ray dose on photoconductivity.

---

[*]XPS = X-ray photoelectron spectroscopy.
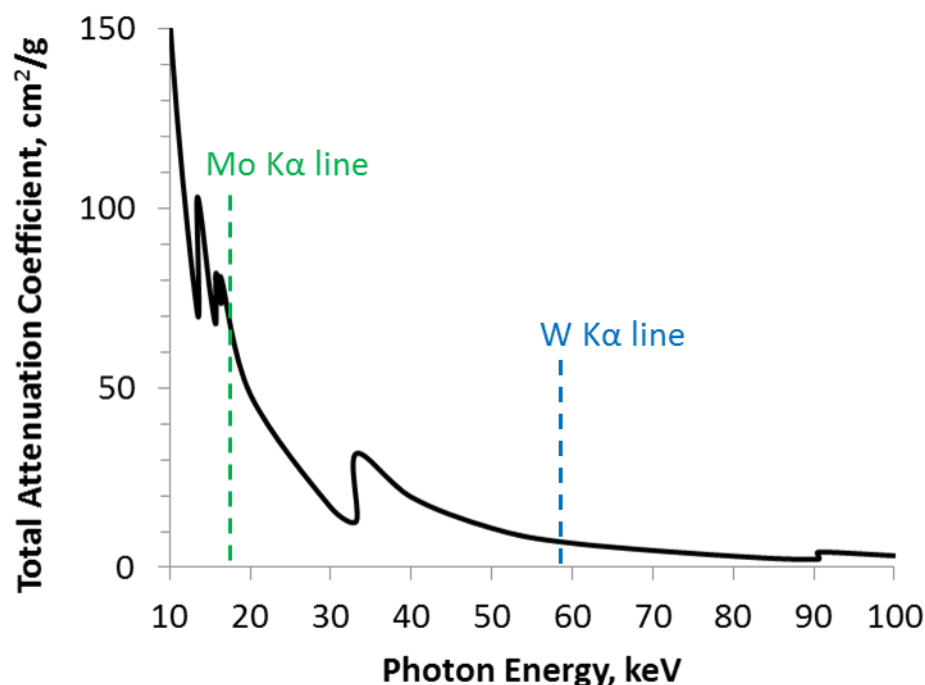
FIGURE 1. BiI$_3$ Attenuation Coefficient as a Function of X-ray Photon Energy.
Kα lines for Mo target and W target are indicated. The X-ray imaging
system used in these efforts had a W target.

Other methods for X-ray detection rely upon interfacial effects rather than bulk interaction in the material. For example, considerable interest has been devoted to X-ray dosimetry using electrets. One such dosimeter design is similar to an ionization chamber in which the externally charged electrode has been replaced with a pre-charged electret. An electret dosimeter does not require an external power supply (References 22 and 23). Ionizing radiation, such as X-rays, produces ions in the airspace thus reducing the voltage of the electret. Besides X-rays, electret ionization chamber-type dosimeters are sensitive to all ionizing radiation including gamma rays and neutrons. Another type of dosimeter design integrates electrets into metal-oxide semiconductor field-effect transistor (MOSFET) X-ray dosimeters (Reference 24). Electrets may be charged by a range of methods including triboelectric, corona charging, thermo-charging, and contact charging. An electret may also be charged by ionizing radiation in air in an external applied field. Aside from dosimetry, electrets also find application in organic field effect transistors for memory application (Reference 25), acoustic sensors and microphones (Reference 26), micropower generators (Reference 27), triboelectric energy generators (Reference 28), metal-insulator-semiconductor (MIS) photovoltaics (Reference 29), and electrically erasable programmable read-only memory (EEPROM) devices (Reference 30).

Literature reports on BiI_3/nylon composites used X-ray sources with a Mo target (Reference 18) or magnesium target (Reference 19). However, W targets are most commonly used in commercial X-ray imaging systems. The spectrum of X-rays emitted from a source depends not only on the element used in the target but also the voltage (Figure 2) (Reference 31). At 40 kilovolts (kV), only the L bands of W are excited, but at 100 kV the K bands are excited also. (Note the scales of the vertical axes are not equal; the intensity in the 100 kV plot is greater than that in the 40 kV across the entire spectrum.) The spectrum of X-rays emitted includes a continuous *bremsstrahlung* radiation with superimposed lines characteristic of the element used in the target (Figure 3) (Reference 32). The maximum photon energy is determined by the voltage accelerating electrons to impact the target (in Figure 3, the voltage was set at 150 kV).
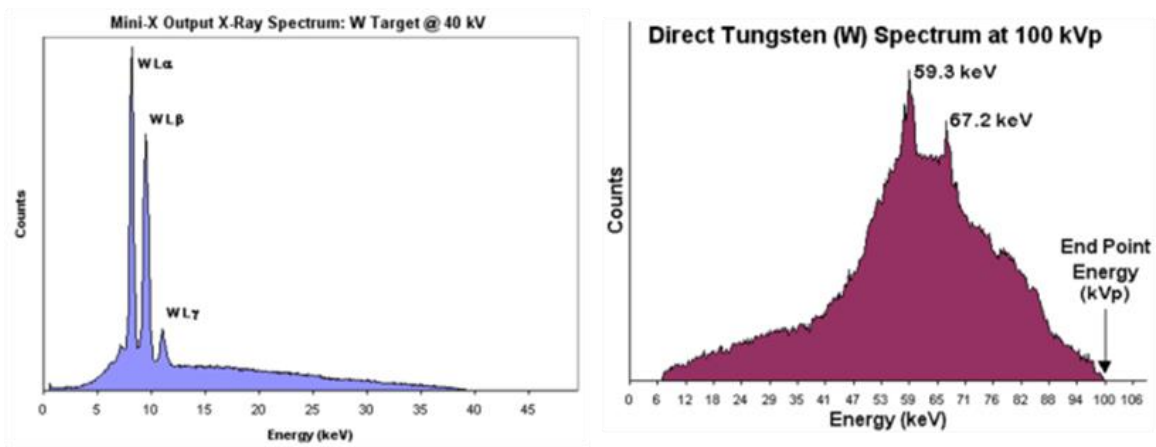
FIGURE 2. X-ray Spectrum From a W Target at 40 kV (left) and 100 kV (right).
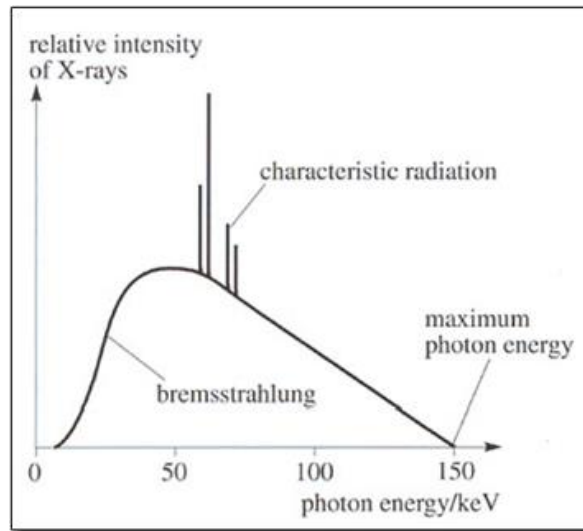
FIGURE 3. Typical Spectrum of X-rays Emitted From a Target.

Aside from X-ray sensitivity, another problem addressed in our projects was the material processing. A method for mixing of the thermoplastic nylon composite was developed. ResonantAcoustic® Mixing (RAM) is a relatively new mixing technology that facilitates component mixing through application of high intensity, low frequency acoustic waves. The localized shear fields that result from the application of the acoustic waves result in bulk flow and mixing. Programs at the Naval Air Warfare Center Weapons Division (NAWCWD) have shown that RAM can quickly and effectively process and mix viscous propellant formulations even when the formulation viscosity would prohibit successful mixing in conventional mechanical mixing technologies; hence, RAM appeared to be a promising technology for nanocomposite mixing. The Resodyn LabRAM mixer as received was not equipped to heat samples to the temperatures necessary for melting the nylon binder (>200°C), so an improvised two-stage mix method was developed.

EXPERIMENTAL METHODS

NANOCOMPOSITE MIXING

Resonant Acoustic Mixes

In order to implement the planned mixing strategy, a high temperature (<300°C) mixing vessel was designed, machined, assembled, and tested at NAWCWD. The mixing vessel was constructed of aluminum (Al) with a removable stainless steel (SS) liner (Figure 4).

In a general procedure, Nylon-11 (Sigma-Aldrich 3-millimeter [mm] pellets, melting point 198°C, dried at 150°C under vacuum for 2 hours) and BiI_3 (Strem, 1- to 20-micrometer [μm] particles) were weighed and sealed inside of the mixing vessel under an inert atmosphere. A dry box was employed to minimize moisture contamination that might cause the BiI_3 component to hydrolyze during elevated temperature mix cycles. The sealed mixing vessel was transferred to a nitrogen (N_2)-purged oven and heated to 230°C for 2 hours. This long thermal soak period allowed ample time for the nylon to completely melt. The mixing vessel was then positioned on top of a precut sheet of ethylene propylene diene monomer (EPDM) rubber and bolted to the platen of the Resodyn LabRAM. The RAM vibrates in a vertical-only motion at 60 hertz (Hz). The applied amplitude was varied until efficient mixing was evident and then held constant for approximately 5 minutes. The total time including bolting the fixture to the LabRAM and mixing was kept below 10 minutes. After mixing, the vessel was unbolted and transferred to a N_2-purged glovebox where the vessel was opened and the SS liner removed for visual inspection of the nanocomposite. Following this inspection, the material appeared to be homogenously mixed after just one mixing cycle. The SS liner was used in subsequent processing.
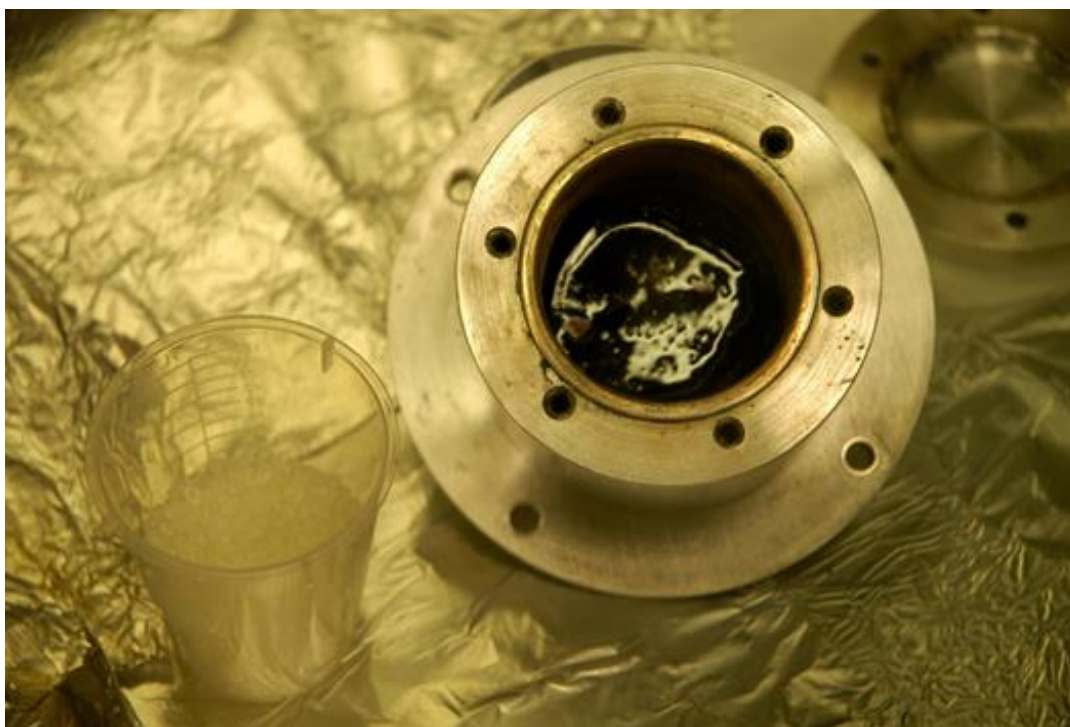
FIGURE 4. Mixing Container Shown With Lid Removed
to Reveal 55% BiI$_3$/45% Nylon-11 Nanocomposite.
The Nylon-11 pellet ingredient is shown in the beaker.

A 40-g sample of 60% BiI$_3$/Nylon-11 was prepared as previously described. The sample appeared to be well mixed but contained some gas bubbles. Heat treatment in an oven at 225°C for 1 hour under N$_2$ reduced the number of bubbles. Additional heating at 210°C under vacuum for 1 hour had little effect. To transfer the sample from the metal mixing container to a 4-inch diameter Al pan, the sample was melted by heating under N$_2$ on a hotplate set to 275°C for 25 minutes then poured into the Al pan. Some smoke came off the sample during this heating, indicating the onset of thermal decomposition. The sample was characterized by X-ray imaging (Figure 5). The X-ray images reveal that most of the sample was well mixed and homogeneous. However, a low concentration of small particles of undissolved BiI$_3$ and small air bubbles remain dispersed throughout the sample.

(a) 6X.   (b) 200X.   (c) Field of view
                                                                    ~ 50 mm x 50 mm.
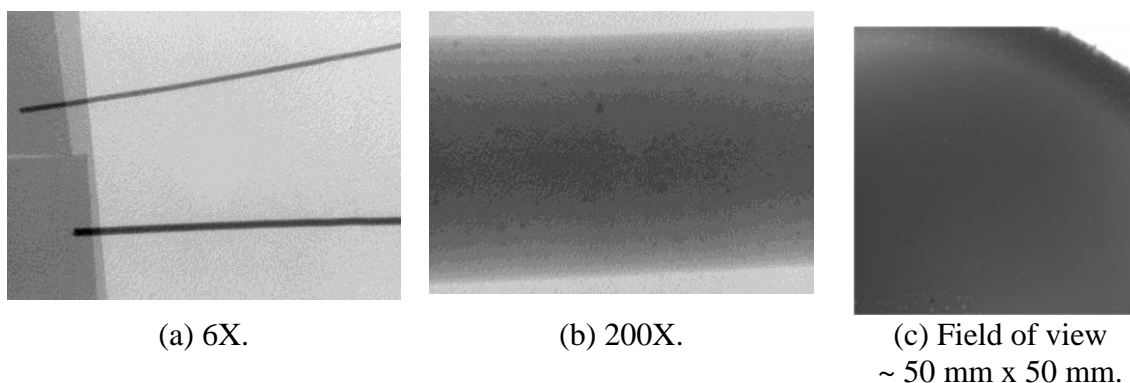
FIGURE 5. X-ray Images of Melt-Pulled Fibers and Pressed Film
Reveal Quality of Mixing of Nanocomposite.

Dry Mixes

As a possible alternative method to Resodyn mixing, several attempts were made to prepare 60% BiI_3/nylon nanocomposite by dry mixing ingredients (ground BiI_3 powder and Nylon-12 powder or Nylon-11 pellets) and then melting the mixture. None of the resulting materials were as homogeneous as the Resodyn mix. Heating and manual mixing of the samples led to thermal decomposition at the temperatures required to give sufficient fluidity for manual mixing.

FILM PROCESSING

Films of BiI_3/Nylon-11 or Nylon-11 were generally melt-pressed between two pieces of Al foil, using ceramic spacers to control film thickness, as shown schematically in Figure 6. The samples are summarized in Table 1. The source material was heated in an Al pan on an Al plate on a hotplate set at 200°C. The hot viscous material (fluid like honey) was transferred by using a glass rod to the Al foil substrate that was also placed on an Al plate on the hotplate. Note that the hotplate temperature was taken to be that indicated by the hotplate. The indicated temperatures corresponded well with the expected softening temperature of the nylon.
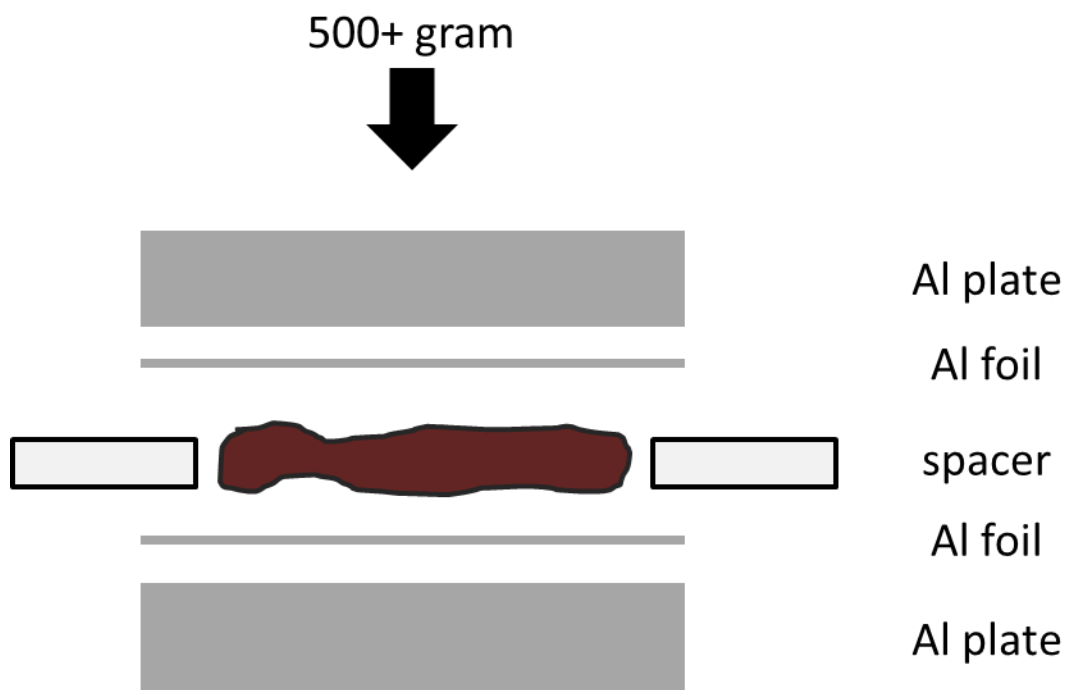
FIGURE 6. Schematic View of Nanocomposite Melt-Press Process.
(See text for details.)

TABLE 1. Melt-Pressed Films – Composition, Thickness, Processing Temperature.

Film	Material	Foil Thickness, μm	Film Thickness, μm	Processing T, °C
1	60% BiI$_3$/Nylon-11	18	25	200
2	60% BiI$_3$/Nylon-11	18	250	200
3	Nylon-11	43	Unknown	220
4	60% BiI$_3$/Nylon-11	43	500	200
5	60% BiI$_3$/Nylon-11	76	500	180
6	60% BiI$_3$/Nylon-11	76	250	180
7	60% BiI$_3$/Nylon-11	76	750 Nominal	180
8	60% BiI$_3$/Nylon-11	No top foil	Self-leveled	170

WOOD-EMBEDDED SAMPLES

Test samples were prepared by forming nanocomposite melt in molds in a N_2-purged glovebox. The molds consisted of half-inch holes drilled partway through a pinewood plank with a small diameter through-hole to facilitate melt filling without trapping air. The wood molds and each nanocomposite were heated on a hotplate to 200°C. Once the nanocomposite melted, a portion was transferred to the molds using a glass rod. The nanocomposite-containing molds were held an additional 10 minutes at 200°C to allow the melt to flow and conform to the mold shape. The hotplate was turned off and the samples cooled slowly to room temperature atop the hotplate.

FLUOROPOLYMER COATING PROCEDURE

Some test samples of 30% BiI_3/nylon were coated with a fluoropolymer using DuPont Teflon® amorphous fluoroplastic (AF) resin in a fluorocarbon solution. A few drops of the solution were applied to samples in the wood mold with the overflow liquid removed with a pipet or by wicking with a tissue. After about 15 minutes, the samples were positioned vertically and allowed to dry overnight at room temperature.

X-RAY EXPOSURE TESTS

All of the X-ray exposure tests were performed using RAM mixed samples or Nylon-11 neat.

Four types of experiments were performed with BiI_3/nylon nanocomposite film samples to test its sensitivity to X-ray exposure: capacitor discharge rate, photoresistor, photochromism, and electrostatic discharge.

Nanocomposite films were exposed to X-rays from two X-ray systems with different power levels.

High Power X-ray Exposure Tests

These experiments used a Comet MXR-320/26 X-ray machine with a maximum power of 4,200 watts specification and 30-degree beam divergence from W target. The Comet machine could be used for imaging of large parts such as rocket motors. Actual voltage and current settings ranged from 40 kilovolts peak (kVp) and 4 milliamperes (mA) up to 320 kVp and 13 mA. The maximum estimated energy flux at 3,840 watts was 4.6 watts per square centimeter (W/cm^2).

We performed a series of experiments where we monitored the discharge of the nanocomposite samples acting as capacitors. A schematic of the test circuit is shown in Figure 7. The 10-megaohm ($M\Omega$) resistor was introduced to increase the time constant

(τ = 4RC) of the circuit to avoid 60 Hz noise. A square wave (1 Hz, 50% duty cycle, 2-volt [V] amplitude, -1 V offset) from an HP 8116A function generator was amplified with a KEPCO bipolar operational power supply/amplifier (voltage mode, voltage control on). With these settings, a 1 Hz voltage square wave oscillating between 0 V and up to 150 V could be applied to the sample. A Tektronix TDS1000 oscilloscope (Measure Fall Time function selected) was used to capture the charge and discharge cycles. A known 100-picofarad (pF) capacitor had a measured fall time of 3.9 milliseconds (ms). Our samples' measured fall times were of the same magnitude as the 100-pF capacitor. A video camera recorded the oscilloscope screen during the X-ray exposures. The nanocomposite film was a dielectric, so it was expected that photoconductive behavior would change the dielectric constant and thus its discharge characteristics during X-ray exposure. However, a series of brief high power X-ray exposures did not result in a significant change (see the following details). The following X-ray exposures were performed:

1. Film **4** (see Table 1) exposed sequentially to 40 kVp/4 mA, 80 kVp/5 mA, 120 kVp/6 mA (first exposure 7 seconds, then 3 seconds); 20 V across sample (~400 volts per centimeter [V/cm]); 100-pF capacitor in circuit. No change noticed in fall time in reviewing video.

2. Film **4** exposed to 260 kVp/13 mA for 10 seconds; 20 V across sample (~400 V/cm); 100-pF capacitor in circuit. No change noticed in fall time.

3. Film **5** exposed to 80 kVp/5 mA, then 260 kVp/13 mA for 10 seconds each; 20 V across sample (~400 V/cm); 100-pF capacitor in circuit. No change noticed in fall time.

4. Film **5** exposed to 80 kVp/5 mA, then 80 kVp/20 mA, then 260 kVp/13 mA for 10 seconds each; 50 V across sample (~1,000 V/cm); 100 pF was not in circuit. No change observed in reviewing video.

5. Film **2** exposed to 80 kVp/5 mA, then 260 kVp/13 mA for 10 seconds each; 50 V across sample (~2,000 V/cm); No change observed in reviewing video.

6. Film **3** (reference) exposed to 80 kVp/5 mA, then 260 kVp/13 mA for 10 seconds each; 50 V across sample. No change observed in reviewing video.
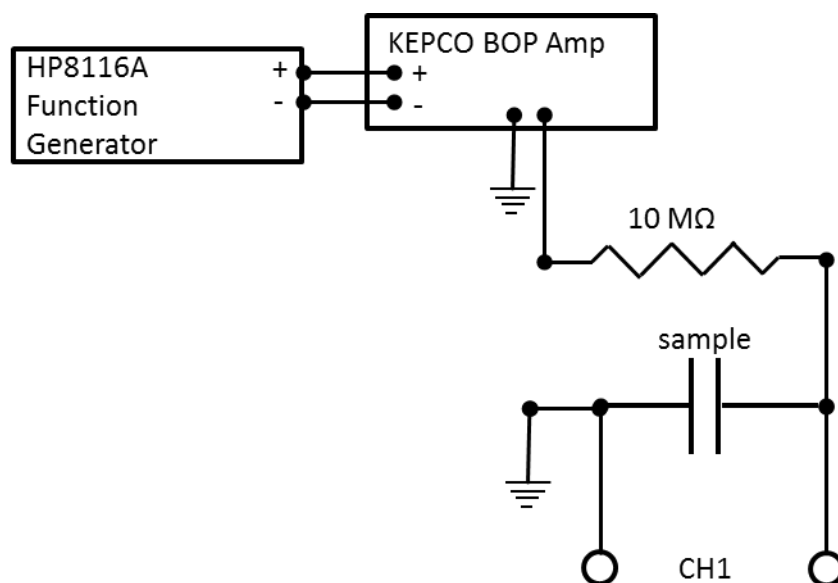
FIGURE 7. Schematic of Circuit for Recording Sample's Capacitor Discharge.

For the X-ray photoresistor experiment, a nanocomposite film with Al electrodes was placed into a standard photoresistor test circuit (Figure 8). While under X-ray exposure, the voltage drop across a current viewing resistor was monitored. Voltage was applied to the samples using the function generator, voltage amplifier, and oscilloscope previously described for the capacitance measurement. Applied voltage was cycled from 0 to 150 V ($\sim$3x10^3 V/cm). After a 7-minute exposure, there was no change in the measured sample resistance.

For the X-ray photochromism experiment, a nanocomposite film under vacuum was exposed to X-rays for 7 minutes (simultaneous experiment with photoresistor test previously mentioned). No change was apparent after X-ray exposure.

For the electrostatic discharge experiments, a charged sample (freestanding nanocomposite film without electrodes) was placed under an electrostatic fieldmeter. The fieldmeter was zeroed at a fixed distance from a wood block and then positioned above the electrostatically charged sample. While under X-ray exposure of 260 kVp and 13 mA, the electrostatic field was monitored. From video screen captures, the time to discharge from -0.20 kilovolt per inch (kV/in) was 0.6 second. The experiment was repeated with similar results.
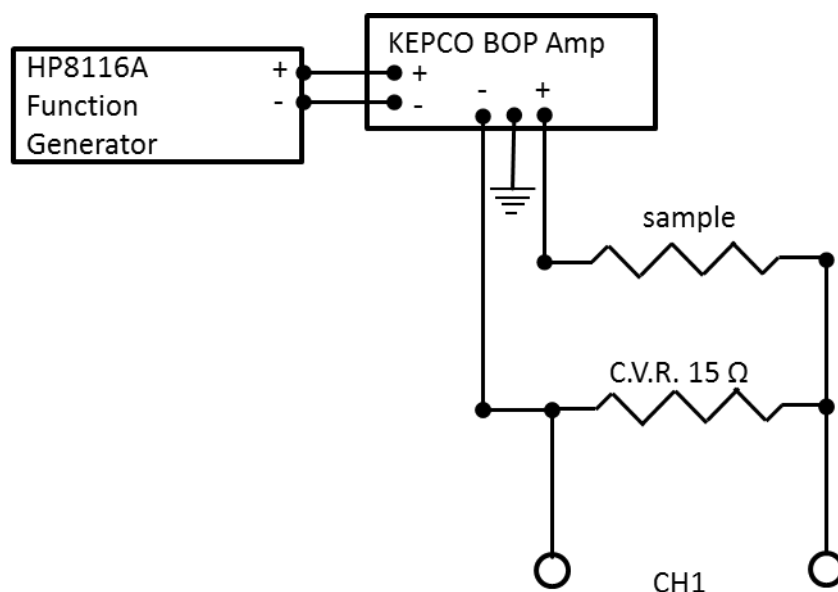
FIGURE 8. Schematic of Circuit for Recording Sample's Resistance Change.

Low Power X-ray Exposure Tests

These experiments used a Metris X-Tek XTV 160 X-ray imaging system. The Metris could be used for imaging small parts such as circuit boards. With the Metris system, typical settings for X-ray imaging are 125 kV and 30 microamperes (μA).

Electrostatic discharge experiments were performed inside the Metris cabinet while the electrostatic voltmeter (Trek Electrostatic Voltmeter Model 821HH Infinitron) monitored the nanocomposite surface charge and the data were stored in a paperless recorder (Monarch Instrument Model DataChart 1250) (Figure 9). Under this X-ray flux, electrostatic discharge of the nanocomposite occurred within seconds (Figure 10). The nanocomposite film was triboelectrically charged by contact with silicone rubber before the film was placed under the voltmeter probe.
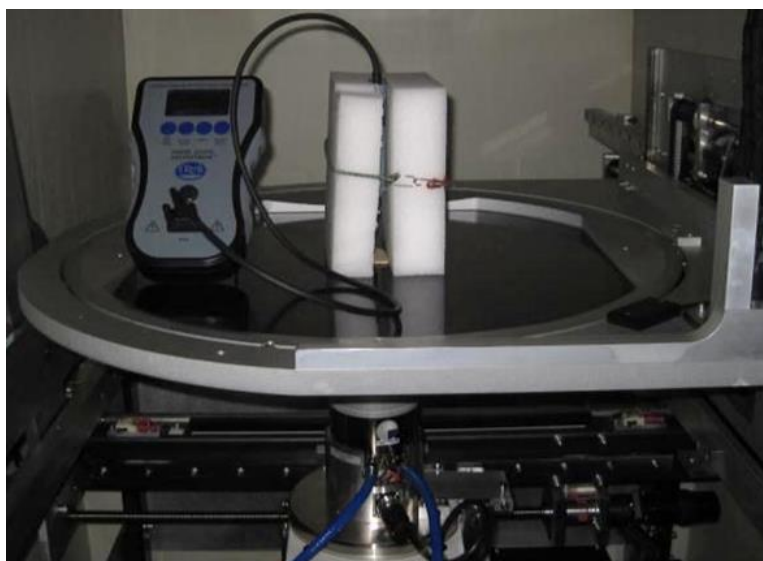
(a) In X-ray imaging system. (Ground strap and paperless recorder not pictured.)

(b) Close-up view of probe and sample.

FIGURE 9. Electrostatic Voltmeter.
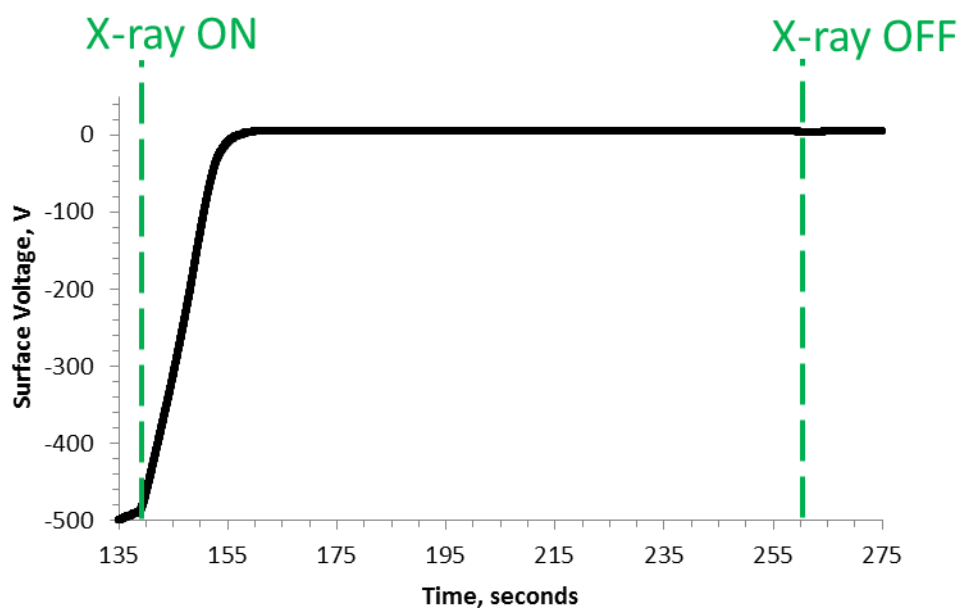
FIGURE 10. Typical Discharge Curve. 60% BiI$_3$/Nylon-11 uncoated, typical imaging, X-ray power settings: 120 kV 30 µA, 45-degree sample orientation, first surface irradiated measured, time to discharge = 21 seconds, average discharge rate = 24 volts per second (V/s), initial discharge rate = 30 V/s.

THERMOGRAVIMETRIC ANALYSIS (TGA)

TGA was conducted under N_2 or air atmosphere with a TA Instruments Q5000 instrument.

RESULTS AND DISCUSSION

Two groups have published on the X-ray effect on BiI_3/nylon nanocomposite. Wang and Herron measured photodischarge of electrostatic voltage at the surface (time scale less than a second) (Reference 18). Zhao et al. measured change in bulk resistance upon long-term exposure (>2 hours) under high vacuum (Reference 19).

In an attempt to see a resistance change (which based on Zhao's results would be a decrease from about 170 to 17 MΩ for our films), we used a relatively long X-ray exposure (8 to 12 minutes to match Zhao's dose) and kept the sample under vacuum during the irradiation. We did not see any resistance or color change. The reason for the contrasting result from the Zhao et al. work is unknown. In Zhao's work, during the reaction of BiI_3 to X-ray, iodine (I_2) was generated. It may be necessary to maintain high vacuum for a long period of time for the I_2 to diffuse out of the nanocomposite; Zhao's vacuum was maintained at $\sim 10^{-9}$ torr during long-term X-ray exposure (our vacuum was no better than 10^{-3} torr).

We also performed a series of experiments in which we monitored the discharge of the nanocomposite samples acting as capacitors. Measurements indicated our samples acted similar to a 100-pF capacitor. As the nanocomposite film was a dielectric, the effect of X-ray exposure may change the dielectric constant and thus its discharge characteristics. However, a series of brief high power X-ray exposures failed to find a significant change.

Lastly, we performed experiments that measured photodischarge of electrostatic voltage at the surface. Without X-ray exposure, the electrostatic charge on the nanocomposite surface decayed within minutes under ambient (~40%) humidity, as expected. Under very low humidity (<5%), the electrostatic charge was constant over several hours.

Discharge experiments were performed under the lower X-ray power Metris system. Five materials were studied for their X-ray induced discharge behavior. The samples consisted of 30, 50, and 60% BiI_3/Nylon-11 nanocomposites, pure Nylon-11, and a fluoropolymer-coated 30% BiI_3/nylon nanocomposite. The fluoropolymer coating was intended to enhance the stability of applied electrostatic charge (Reference 30). Figure 11 shows a radiographic image of nanocomposite samples that were formed in the mold. The bright circular spots in both images are attributed to small (<1 mm) gas bubbles in the film.
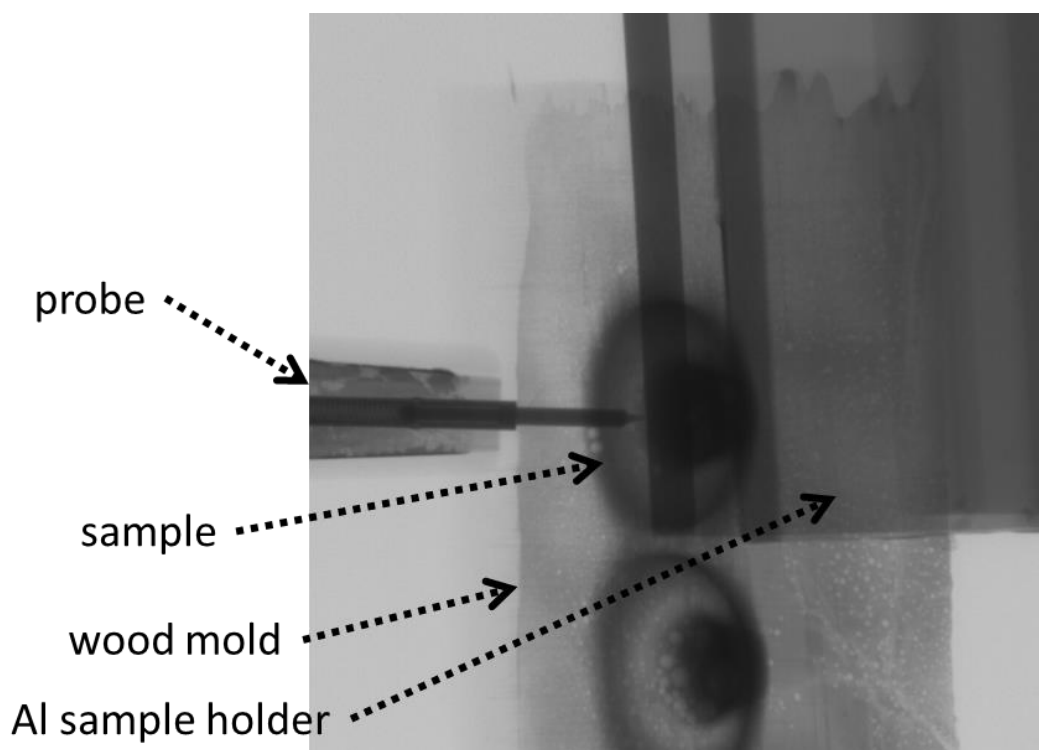
FIGURE 11. X-ray Radiograph of Nanocomposite Sample in the 45-Degree Orientation.

All samples were charged triboelectrically via contact with silicone rubber. This charging method has important advantages of convenience and does not require special charging apparatus. The disadvantages of tribo-charging are that there is less control over the resulting surface charge because it depends on the relative position in the triboelectric series (see Table 2; Reference 33) and that the surface charge obtained is less reproducible. The reproducibility was found to be improved by using an unused piece of silicone rubber to charge each sample.

TABLE 2. Triboelectric Series With Selected Materials (Reference 33).

Most Positively Charged	Most Negatively Charged
Polyurethane foam	Ebonite
Nylon	Silicone rubber
Glass	Teflon
Leather	Polyethylene (like Scotch tape)
Silk	Polyester
Aluminum	Rubber balloon
Paper (small positive charge)	Wood (small negative charge)
Wool (no charge)	Steel (no charge)

A typical X-ray induced discharge curve is shown in Figure 10. The results from many sample tests are summarized in Figure 12 and Table 3. The initial surface charge was positive for nylon and the fluoropolymer coated nanocomposite sample, consistent with the triboelectric series. The uncoated nanocomposite samples initially had a negative charge, indicating a strong influence of BiI_3 on the nanocomposite surface properties.

The 30 weight percent (wt%) BiI_3 concentration samples have more negative surface charge after triboelectric charging compared to the 50 and 60% samples. This result suggests that the 30% samples remove more electrons from silicone. In principle, it should be possible to control the polarity of the charge by using different materials on the triboelectric series; however, this was not attempted in this project.

Figure 12 shows a general trend of faster initial discharge rate, $(dQ/dt)_{init}$, for higher surface voltage (either positive or negative), regardless of the BiI_3 concentration or the presence of a surface coating. Even pure nylon samples discharged rapidly. Higher power X-ray settings gave faster discharge for all samples, as expected and providing a level of confidence in the data.
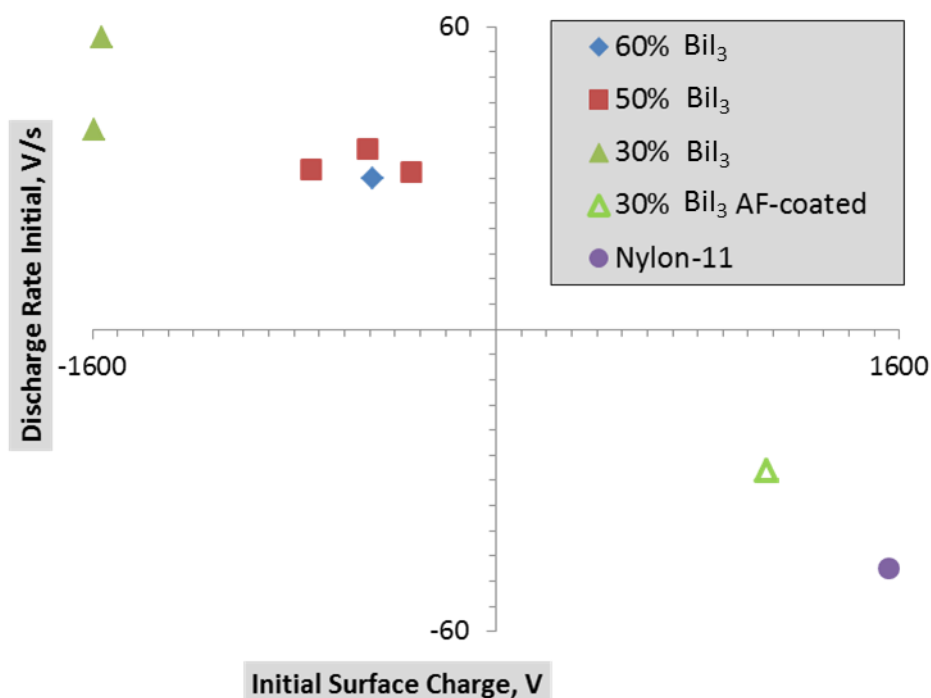

FIGURE 12. Summary Plot of Initial Discharge Rate in Ambient Air as a Function of Initial Surface Charge. X-ray settings: 120 kV, 30 µA.

TABLE 3. Measurements of X-ray Exposure Effect on Surface Voltage.

Sample	X-ray Settings	Initial Surface Charge, V	Time to Discharge, s	Discharge Rate Initial, V/s	Discharge Rate Average, V/s
60% BiI$_3$	No X-ray, ambient	-180	>120	0.3	0.2
60% BiI$_3$	120 kV, 30 μA, 45 degrees	-489	21	30	24
50% BiI$_3$	70 kV, 30 μA	-590	112	7.5	5.2
50% BiI$_3$	120 kV, 30 μA	-734	18	31.8	40
50% BiI$_3$	120 kV, 30 μA	-336	15	31.3	22.7
50% BiI$_3$	120 kV, 30 μA	-511	18	35.9	29.5
50% BiI$_3$	120 kV, 30 μA, 45 degrees	-1,200	31	57	38
30% BiI$_3$	70 kV, 30 μA	-1,257	130	9.6	9.5
30% BiI$_3$	120 kV, 30 μA	-1,561	26	58	62
30% BiI$_3$	120 kV, 30 μA	-1,591	40	39.6	40.7
30% BiI$_3$	120 kV, 30 μA, 45 degrees	-1,507	24	80.4	62.8
30% BiI$_3$ AF-coated	70 kV, 30 μA	112	76	-4.5	-1.4
30% BiI$_3$ AF-coated	120 kV, 30 μA	1,072	28	-28	-35
30% BiI$_3$ AF-coated	120 kV, 30 μA, 45 degrees	417	10	-52	-40
Nylon-11	120 kV, 30 μA	1,557	28	-47.4	-57.7
Nylon011	120 kV, 30 μA, 45 degrees	775	9	-93	-90

The rapid discharge of the pure nylon samples was attributed to free charges in the air generated by the ionizing effect of X-ray radiation (Reference 26). The data indicated that free charges generated in air are also the dominant process causing discharge of the BiI$_3$/nylon samples (Figure 13). As can be seen in Figure 12, the $(dQ/dt)_{init}$ was roughly proportional to the initial surface charge. The mobility of free charges in air is much greater than the charge mobility within the nanocomposite.
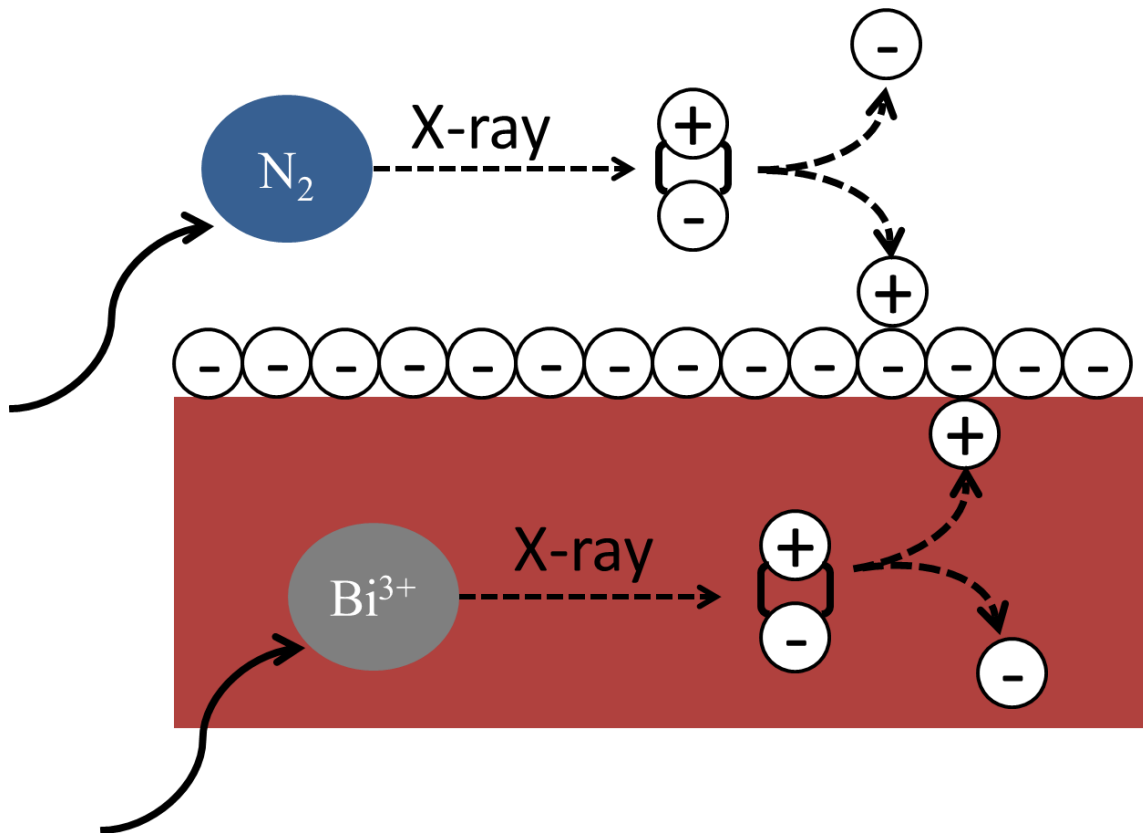
FIGURE 13. Competing Processes in X-ray Induced Discharge
of Surfaces in Contact With Air.

To examine whether X-ray absorption by BiI_3 plays a role in the X-ray induced discharge, we performed tests in the presence of isopropyl alcohol (IPA) vapor, which acts to quench free charges in the gas phase (Reference 33). As can be seen in Figure 14, IPA vapor has an effect on $(dQ/dt)_{init}$. The magnitude of $(dQ/dt)_{init}$ for Nylon-11 is decreased from -47 to -7 V/s. Yet more information may be gleaned by comparing the $(dQ/dt)_{init}$ of Nylon-11 and nanocomposite samples (Table 4). In the presence of IPA vapor, the $(dQ/dt)_{init}$ of the N-11 is as low or lower than the $(dQ/dt)_{init}$ for any of the nanocomposite samples. This is true even for nanocomposite samples with much lower initial charge. These data suggest that the BiI_3 content does contribute to the surface discharge. The 30 wt% BiI_3 nanocomposite appears to have the best overall performance in this study, due to its ability to maintain a higher initial surface charge.
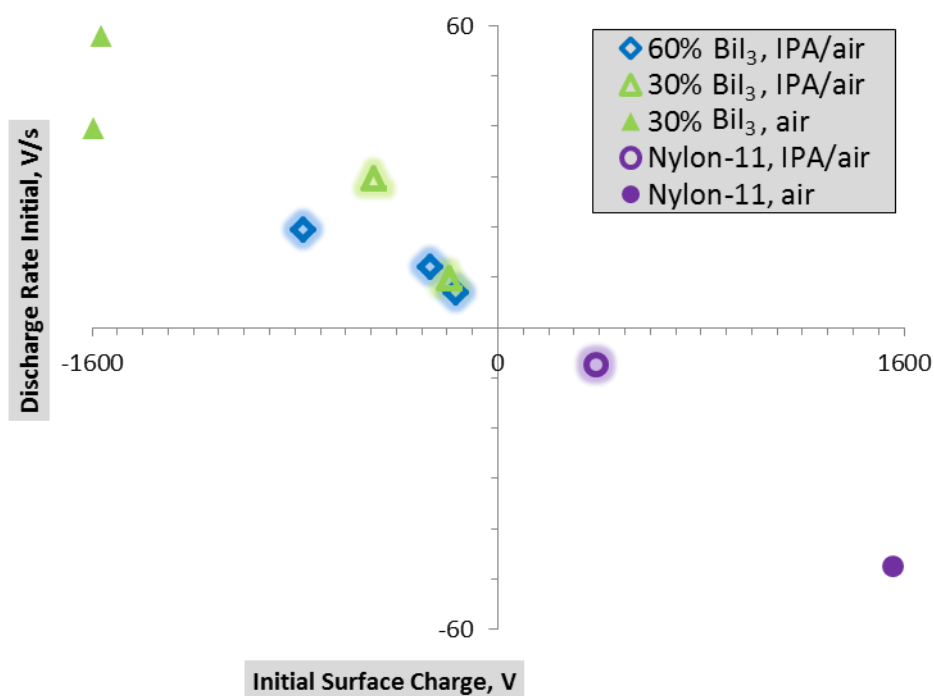
FIGURE 14. Plot of Initial Discharge Rate as a Function of Initial
Surface Charge for Samples Under IPA Vapor Atmosphere.

TABLE 4. Discharge Data for Samples Under IPA Vapor Atmosphere and Under Air.

All data in this table were taken with X-ray settings 120 kV, 30 µA.

Sample	Atmosphere	Initial Surface Charge, V	Time to Discharge, s	Discharge Rate Initial, V/s
Nylon-11	Air	1,557	28	-47.4
Nylon-11	IPA/air	384	120	-7.3
30% BiI$_3$	Air	-1,561	26	58
30% BiI$_3$	Air	-1,591	40	39.6
30% BiI$_3$	IPA/air	-489	21	29.6
30% BiI$_3$	IPA/air	-194	44	9.8
60% BiI$_3$	IPA/air	-268	108	12
60% BiI$_3$	IPA/air	-166	39	7.1
60% BiI$_3$	IPA/air	-768	111	19.4

A report on X-ray photoconductive nanocomposites (Reference 18) was the initial inspiration for much of the work we performed on the X-ray sensitive materials. A close reading of their method for measuring X-ray photoconductivity does not reveal whether they have accounted for the effect of free-charges generated in air. Electrets can be made more sensitive by replacing the air with a gas with lower free-charge generation energy, such as argon (Reference 26); conversely, replacing air with a free-charge quenching gas such as butane or ethanol lowers the sensitivity. However, it appears that the Wang and Herron report does not account for such free-charge generation in air by X-rays. The Wang and Herron report does not provide data showing photocurrent generation. Reports on other X-ray photoconductors, such as amorphous selenium, typically show such data (Reference 34). We looked for evidence of photocurrent in BiI_3/Nylon-11 thin films but found none even under very high X-ray flux and cumulative dose. Data indicate that BiI_3 content does contribute to surface discharge; however, further work is warranted to measure the photocurrent. Selenium films used for photocurrent measurements were typically 150 to 320 μm thick and our samples have been 250 to 750 μm thick. Photocurrent measurements of selenium films required applied voltage in the range of 10^4 to 10^5 V/cm (Reference 34). In comparison, our applied voltages were $\sim10^3$ V/cm.

The long-term stability of surface charge was measured under ambient and under low humidity conditions (<3% relative humidity). Under ambient conditions, a 60 wt% sample charged to -1,100 V dropped to near 0 V within 5 minutes. Under low humidity conditions, the same sample charged to -1,500 V dropped to -1,450 V in 5 minutes. Under low humidity conditions, a 30 wt % AF-coated sample charged to 250 V dropped to 50 V during 14 hours (Figure 15).

In thermal analysis experiments (Figure 16), the 60% BiI_3 nanocomposite showed good thermal stability, with <0.5% weight loss after heating at 180°C for 120 minutes under N_2. At 200°C, the nanocomposite lost 3.1 wt % during 8 hours under N_2.
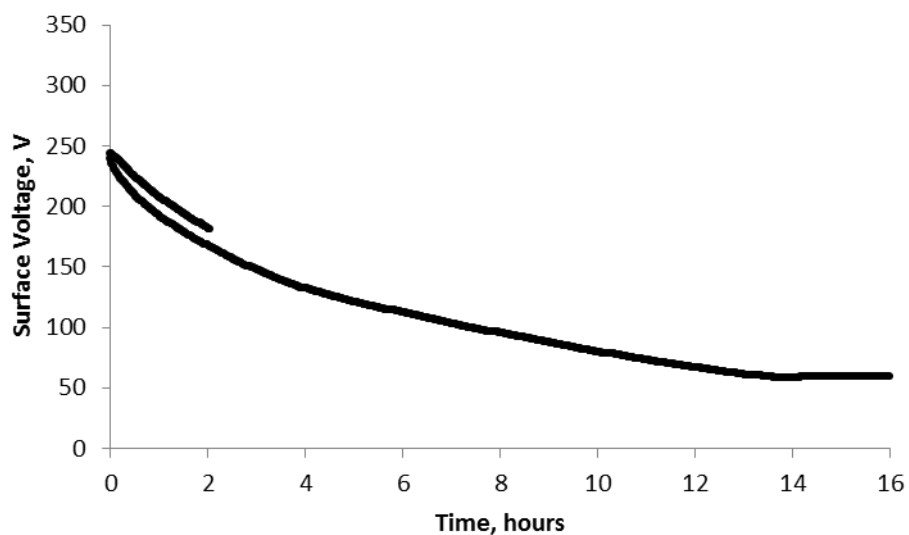
FIGURE 15. Evolution of Surface Charge Over Time for a
30% BiI$_3$/Nylon-11 AF-Coated Sample in Dry N$_2$ Atmosphere.
Two tests are shown: one for 2-hour period
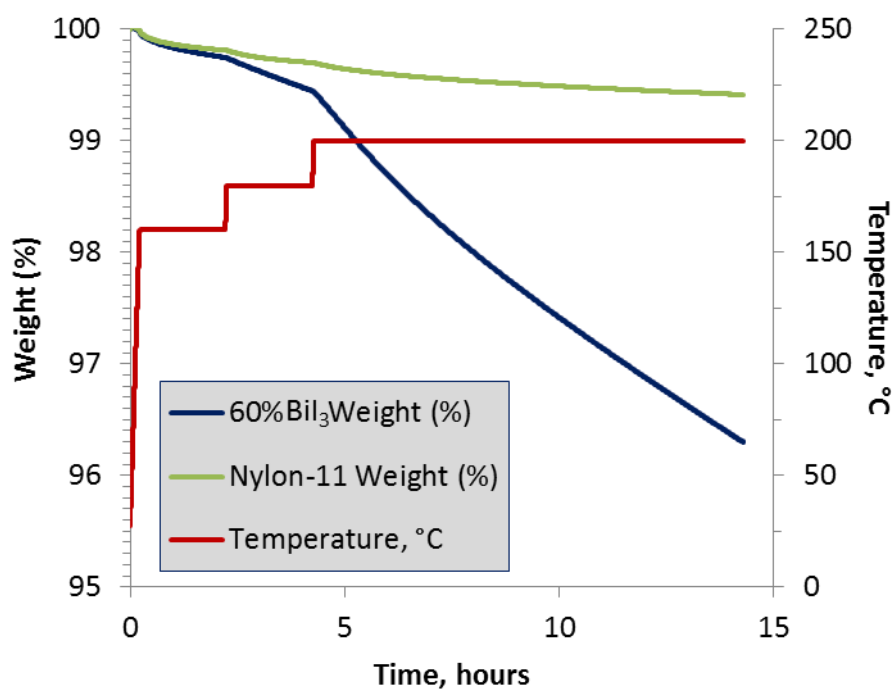and the other for 16 hours.

FIGURE 16. TGA of 60 wt% BiI$_3$ Nanocomposite Compared With Pure Nylon-11.

SUMMARY

In these studies, excellent mixing of BiI_3/Nylon-11 nanocomposites was achieved with a resonant acoustic mixer. The nanocomposites were melt-processed into fibers, molded discs, and pressed films. The effect of X-ray exposure on the nanocomposite was studied. These studies have established that BiI_3/Nylon-11 nanocomposites were sensitive to X-ray from W sources.

In conclusion, the BiI_3/nylon-11 nanocomposite may be useful in X-ray induced discharge applications in controlled environments. The tasks completed include

1. Prepared well-mixed BiI_3/nylon-11 nanocomposite samples (60, 50, 30% BiI_3).

2. Measured the electrostatic charge decay of nanocomposite samples under ambient conditions and under very low humidity.

3. Established that complete electrostatic discharge occurs at minimum X-ray power level necessary for X-ray imaging.

4. Characterized the X-ray response versus nanocomposite composition (60, 50, and 30% BiI_3) under ambient air and under IPA/air atmosphere.

5. Investigated thin electret laminate (via fluoropolymer coating) to enhance the stability of the electrostatic charge.

6. Characterized the thermal stability of nanocomposites.

Possible future work includes

1. Fluoropolymer coating may be more effective on the 60% or 50% BiI_3 materials since these had lower initial surface charge and they are better absorbers of X-rays. Also direct comparison of long-term surface charge stability of AF-coated versus uncoated samples is needed to access the effectiveness of AF coating.

2. Differential scanning calorimetry (DSC) of samples to characterize effect of BiI_3 on melting and thermal behavior of nylon composites.

3. X-ray discharge experiments under vacuum to more clearly assess the effect of X-ray absorption of BiI_3 on surface discharge.

4. Use different materials in the triboelectric series to explore modification of the surface charge and effect on discharge behavior.

5. Consider possible utility of X-ray sensitive materials where surface charge is discharged by the mechanism involving free charge generation in the ambient gas (Reference 6). The ambient gas (e.g., dry N_2) could be hermetically sealed if necessary.

6. Quantify the effect of ionizing radiation other than X-ray, such as, gamma rays, etc., since inadvertent exposure may cause a false positive.

7. Application of higher voltages to samples to look for evidence of photocurrent under the influence of X-rays.

NOMENCLATURE

°C	degrees Celsius
AF	amorphous fluoroplastic
Al	aluminum
BiI_3	bismuth(III) iodide
CdZnTe	cadmium zinc telluride
cm^2/g	square centimeters per gram
$(dQ/dt)_{init}$	initial discharge rate
DSC	differential scanning calorimetry
EEPROM	electrically erasable programmable read-only memory
EPDM	ethylene propylene diene monomer
FY	fiscal year
g	grams
HgI_2	mercury(II) iodide
Hz	hertz
I_2	iodine
IPA	isopropyl alcohol
keV	kiloelectron volts
kV	kilovolts
kV/in	kilovolt per inch
kVp	kilovolts peak
mA	milliamperes
MIS	metal-insulator-semiconductor
mm	millimeters
Mo	molybdenum
MOSFET	metal-oxide semiconductor field-effect transistor
ms	milliseconds
$M\Omega$	megaohm
N_2	nitrogen
NAWCWD	Naval Air Warfare Center Weapons Division

PbI$_2$	lead(II) iodide
pF	picofarads
RAM	ResonantAcoustic® Mixing
s	seconds
Si	silicon
SS	stainless steel
TGA	thermogravimetric analysis
TlBr	thallium bromide
V	volts
V/cm	volts per centimeter
V/s	volts per second
W	tungsten
W/cm^2	watts per square centimeter
wt%	weight percent
XPS	X-ray photoelectron spectroscopy
μA	microamperes
μm	micrometers

REFERENCES

1. Larry E. Antonuk, Youcef E1-Mohri, Kyung-Wook Jee, Qihua Zhao, Amit Sawant, and Zhong Su. "Technological Pathways for 21st Century Active Matrix X-Ray Imager Development," Medical Imaging 2002: Physics of Medical Imaging, edited by Larry E. Antonuk, Martin J. Yaffe. *Proceedings of SPIE*, Vol. 4682, 1-8 (2002).

2. Azaree T. Lintereur, Wei Qiu, Juan C. Nino, and James E. Baciak. "Iodine Based Compound Semiconductors for Room Temperature Gamma-Ray Spectroscopy," Optics and Photonics in Global Homeland Security IV, edited by Craig S. Halvorson, Daniel Lehrfeld, Theodore T. Saito. *Proceedings of SPIE,* Vol. 6945, 694503, 1-10 (2008).

3. Donald R. Ouimette, Robert M. Lodice, Pang-Jen Kung, and Lahmer Lynds. "A Real-Time X-Ray Image Sensor Using s Thallium Bromide Photoconductor," *SPIE Conference on Medical Applications of Penetrating Radiation*, Denver, Colorado, July 1999, SPIE Vol. 3770, 156-163 (1999).

4. James G. Mainprize, Nancy L. Ford, Shi Yin, Tümay Tümer, Eli Gordon, William J. Hamilton, and Martin J. Yaffe. "Semiconductor Materials for Digital Mammography," Medical Imaging 2000: Physics of Medical Imaging, edited by James T. Dobbins III, John M. Boone. *Proceedings of SPIE*, Vol. 3977, 152-158 (2000).

5. Koichi Ogusu, Osamu Nakane, Yasunori Igasaki, Yoshinori Okamura, Satoshi Yamada, and Tadaaki Hirai. "Advanced a-Se Film With High Sensitivity and Heat-Resistance for X-ray Detectors," Medical Imaging 2009: Physics of Medical Imaging, edited by Ehsan Samei, Jiang Hsieh. *Proceedings of SPIE,* Vol. 7258, 72583M, 1-10 (2009).

6. M. H. Izadi, O. Tousignant, M. Feuto Mokam, M. Yazdandoost, N. Safavian, H. Mani, L. Laperriere, and K. S. Karim. "Performance of a Prototype Amorphous Silicon Active Pixel Sensor Array Using a-Se for Direct X-ray Conversion," Medical Imaging 2010: Physics of Medical Imaging, edited by Ehsan Samei, Norbert J. Pelc. *Proceedings of SPIE,* Vol. 7622, 76223V, 1-10 (2010).

7. Jungwon Kang, Hyungsup Shin, Sangjun Lee, Kisung Lee, and Hakjae Lee. "X-ray Detection Method for the Direct-Conversion Plasma Detector," Hard X-Ray, Gamma-Ray, and Neutron Detector Physics XII, edited by Arnold Burger, Larry A. Franks, Ralph B. James. *Proceedings of SPIE,* Vol. 7805, 78051D, 1-6 (2010).

8. Akarin Intaniwet, Christopher A. Mills, Paul J. Sellin, Maxim Shkunov, and Joseph L. Keddie. "Achieving a Stable Time Response in Polymeric Radiation Sensors Under Charge Injection by X-rays," *ACS Applied Materials and Interfaces*, Vol. 2, No. 6, 1692-1699 (2010).

9. Beatrice Fraboni, Andrea Ciavatti, Francesco Merlo, Luca Pasquini, Anna Cavallini, Alberto Quaranta, Annalisa Bonfiglio, and Alessandro Fraleoni-Morgera. "Organic Semiconducting Single Crystals as Next Generation of Low-Cost, Room-Temperature Electrical X-ray Detectors," *Advanced Materials*, 24, 2289–2293 (2012).

10. A. Intaniwet, C. A. Mills, M. Shkunov, P. J. Sellin, and J. L. Keddie. "Heavy Metallic Oxide Nanoparticles for Enhanced Sensitivity in Semiconducting Polymer X-Ray Detectors," *Nanotechnology* 23, 235502, 1-7 (2012).

11. Ferdi Karadas, Gulay Ertas, Eda Ozkaraoglu, and Şefik Süzer. "X-ray-Induced Production of Gold Nanoparticles on a SiO_2/Si System and in a Poly(methyl methacrylate) Matrix," *Langmuir*, 21, 437-442 (2005).

12. Şefik Süzer. "XPS Investigation of X-Ray-Induced Reduction of Metal Ions," *Applied Spectroscopy*, Vol. 54, No. 11, 1716-1718 (2000).

13. Şefik Süzer. "Deposition and Stability of Metal Ions on Oxidised Silicon Surfaces: Electrochemical Correlation," *Journal of Electron Spectroscopy and Related Phenomena*, 114–116, 1151–1154 (2001).

14. R. Divan, Q. Ma, D.C. Mancini, and D. T. Keane. "Controlled X-Ray Induced Gold Nanoparticles Deposition," *Romanian Journal of Information Science and Technology*, Vol. 11, No. 1, 71-84 (2008).

15. Qing Ma, Nicolaie Moldovan, Derrick C. Mancini, and Richard A. Rosenberg. "Synchrotron-Radiation-Induced, Selective-Area Deposition of Gold on Polyimide From Solution," *Appl. Phys. Lett.*, 76, 2014 (2000).

16. T. Caruso, R. G. Agostino, G. Bongiorno, E. Barborini, P. Piseri, P. Milani, C. Lenardi, S. La Rosa, and M. Bertolo. "Writing Submicrometric Metallic Patterns by Ultraviolet Synchrotron Irradiation of Nanostructured Carbon and TiO_x–Carbon Films," *Applied Physics Letters*, Vol. 84, No. 17, 3412-3414 (2004).

17. Nicola Poccia, Michela Fratini, Alessandro Ricci, Gaetano Campi, Luisa Barba, Alessandra Vittorini-Orgeas, Ginestra Bianconi, Gabriel Aeppli, and Antonio Bianconi. "Evolution and Control of Oxygen Order in a Cuprate Superconductor," *Nature Materials*, Vol. 10, 733-736 (2011).

18. Y. Wang and N. Herron. "X-Ray Photoconductive Nanocomposites," *Science,* 273, 632-634 (1996).

19. Z. Zhao, F. Liu, L. Zhao, and S. Yana. "XPS Study on BiI_3–nylon 11 Nanocomposites," *Materials Chemistry and Physics,* 124, 55–59 (2010).

20. "XCOM: NIST Photon Cross Sections Database," accessed 23 November 2015, http://www.nist.gov/pml/data/xcom/index.cfm

21. Robert C. Weast. *Handbook of Chemistry and Physics*. 61st edition. Taipei: Ta Tung Book/Chemical Rubber Co., 1981. Pp. D-155 to D-160.

22. G. Pretzsch, B. Dorschel, and T. Schonmuth. *IEEE Transactions on Electrical Insulation,* Vol. EI-21, No.3, June 1986, pp. 437-441.

23. C. Son and B. Ziaie. "A Micromachined Electret-Based Transponder for In Situ Radiation Measurement," *IEEE Electron Device Letters*, Vol. 27, No. 11, 884-886 (2006).

24. D. R. Ciarlo. "MOSFET Detector Evaluation," *IEEE Transactions on Nuclear Science*, Vol. 21, Issue 1, pp. 390-394 (1974).

25. H. Chi, H. Hsu, S. Tung, and C. Liu. "Nonvolatile Organic Field-Effect Transistors Memory Devices Using Supramolecular Block Copolymer/Functional Small Molecule Nanocomposite Electret," *ACS Appl. Mater. Interfaces*, 7, 5663−5673 (2015).

26. G. M. Sessler, ed. *Electrets*, 3rd Edition, Volume 1. Laplacian Press, Morgan Hill, California, 1998. Pp. 400-401, 405-407.

27. Y. Sakane, Y. Suzuki, and N. Kasagi. "The development of a high-performance perfluorinated polymer electret and its application to micro power generation," *J. Micromech. Microeng.,* 18, 104011 (2008).

28. Y. Yang, H. Zhang, X. Zhong, F. Yi, R. Yu, Y. Zhang, and Z. L. Wang. "Electret Film-Enhanced Triboelectric Nanogenerator Matrix for Self-Powered Instantaneous Tactile Imaging," *ACS Appl. Mater. Interfaces*, dx.doi.org/10.1021/am406018h.

29. J. E. Klemberg-Sapieha, L. Martinu, M. R. Wertheiryier, P. Gunther, R. Schellin, C. Thielemann, and G. M. Sessler. *J. Vac. Sci. Technol. A,* 14(5), 2775-2779 (1996).

30. M. Kim, N. Y.-M. Shen, C. Lee, and E. C. Kan. "Fast and Sensitive Electret Polymer Characterization by Extended Floating Gate MOSFET," *IEEE Trans. Dielectr. Electr. Insul.,* Vol. 12, No. 5, 1082-1087 (2005).

31. "Amptek," accessed 20 October 2015, http://www.amptek.com/medical.html

32. "Spectrum of the X-rays Emitted by an X-ray Tube With a Tungsten Target," accessed October 2012, labspace.open.ac.uk

33. "Triboelectric Effect," *Wikipedia*, last modified 26 October 2015, http://en.wikipedia.org/wiki/Triboelectric_effect

34. J. L. Donovan. "X-ray Sensitivity of Selenium," *J. Appl. Phys.,* Vol. 50, No. 10, 6500-6504 (1979).

INITIAL DISTRIBUTION

1   Naval Surface Warfare Center Crane Division, Crane, IN (Crum, D.)
1   Defense Technical Information Center, Fort Belvoir, VA

_____

ON-SITE DISTRIBUTION

2   Code 4F0000D
       Johnson, C.
       Roberts, M. J.
4   Code 4G0000D (archive and file copies)
1   Code 41Q000D, Harlow, J.